SCIENCE CHINA Earth Sciences



·ARTICLE ·

October 2025 Vol.68 No.10: 3385–3394 https://doi.org/10.1007/s11430-025-1662-7

Regional contributions to gross primary productivity changes across the Tibetan Plateau and climate attribution

Mengzi ZHOU¹, Guangsheng ZHOU^{1,2*} & Li ZHOU¹

Received April 27, 2025; revised August 7, 2025; accepted August 13, 2025; published online September 22, 2025

Abstract As a critical region sensitive to global warming, the ecosystem dynamics of the Tibetan Plateau are regulated by the interaction between the westerlies and monsoon circulation systems. Utilizing remote sensing observations, this study quantifies the relative contributions of three climatic zones (monsoon, transition, and westerlies) to the evolution of gross primary productivity (GPP) and identifies their respective climatic drivers. Results reveal that while the monsoon zone dominates the plateau-wide GPP for the mean state (86.07%), long-term trend (69.84%), and interannual variability (81.80%), its relative contributions to GPP changes (i.e., long-term trends and interannual variability) are proportionally lower than to the mean state. Conversely, both the transition and westerlies zones exhibit proportionally higher contributions to GPP changes relative to their mean-state contributions. Temperature is the primary driver of the long-term GPP increase across the Tibetan Plateau and its subregions, though with a weaker contribution rate (57.26%) in the transition zone compared with the monsoon (77.88%) and westerlies zones (71.35%). The interannual variability of GPP across both the entire plateau and its subregions is also dominated by temperature, yet process-based ecosystem models fail to replicate this dominant temperature control. Our study elucidates complex GPP-climate interactions under the westerlies-monsoon synergy, highlighting the imperative to improve model parameterization for accurately capturing interannual variability in alpine ecosystem dynamics.

Keywords GPP, Long-term trend, Interannual variability, Relative contribution, Tibetan Plateau

Citation: Zhou M, Zhou G, Zhou L. 2025. Regional contributions to gross primary productivity changes across the Tibetan Plateau and climate attribution. Science China Earth Sciences, 68(10): 3385–3394, https://doi.org/10.1007/s11430-025-1662-7

1. Introduction

Terrestrial ecosystems serve as a critical carbon sink, mitigating rising atmospheric CO_2 through the balance between gross primary production (GPP) and carbon release processes (e.g., ecosystem respiration and wildfires). Over the past decade, terrestrial carbon sequestration has offset ~29% of anthropogenic carbon emissions annually (Friedlingstein et al., 2022). As the foundation of the ecosystem carbon cycle, GPP governs initial matter and energy inputs into

ecosystems. Even minor changes in GPP can significantly alter carbon budgets (Yao et al., 2018) and trigger climate feedbacks (Baldocchi et al., 2018). Consequently, accurately assessing spatiotemporal dynamics of GPP and its driving factors is crucial for informing climate change mitigation strategies (Li et al., 2021).

The Tibetan Plateau (TP), known as the "Roof of the World", is the highest and most extensive highland in the world. The climate system is governed by the westerlies and Asian monsoon system, making it highly sensitive to global climate change (Yao et al., 2012). The synergistic effects of the westerlies and monsoon shape the unique ecological

¹ State Key Laboratory of Severe Weather Meteorological Science and Technology, Chinese Academy of Meteorological Sciences, Beijing 100081, China

² Collaborative Innovation Center on Forecast and Evaluation of Meteorological Disasters, Nanjing University of Information Science and Technology, Nanjing 210044, China

^{*} Corresponding author (email: zhougs@cma.gov.cn)

patterns of the TP through modulation of regional thermodynamic and dynamic conditions. Based on the spatial heterogeneity of atmospheric circulation systems, Yao et al. (2013) roughly divided the TP into three typical climatic subregions along 30°N and 35°N: the westerlies, the monsoon, and the transition zones. The westerlies zone, primarily regulated by the mid-latitude westerlies, features cold, arid desert ecosystems with spatially uniform low GPP. In contrast, the monsoon zone receives abundant precipitation from both South Asian (Maussion et al., 2014) and East Asian monsoons (Zhang et al., 2017), sustaining dense vegetation that dominates plateau-wide GPP. The transition zone exhibits complex bioclimatic characteristics due to interactions of these circulation systems. Notably, beyond the mean state, GPP dynamics encompass two critical temporal dimensions: long-term trend and interannual variability (IAV). Long-term trends reflect the integrated effects of all forcings over extended periods, while interannual variability primarily characterizes year-to-year variations driven by climate fluctuations (Yao et al., 2018). However, regional contributions of these climatic zones to the long-term trends and interannual variability of plateau-wide GPP remain unquantified, hindering the advancement theoretical framework for the carbon cycle in high-altitude ecosystems.

The TP has experienced accelerated warming in recent decades, with trends exceeding the global mean (You et al., 2021). Concurrently, precipitation patterns across TP have shown pronounced regional differences (Li et al., 2021; Liu et al., 2021). As primary regulators of TP GPP, temperature and precipitation modulate physiological and biogeochemical processes (Yao et al., 2018; Wu et al., 2021; Shi et al., 2023). Rapid warming generally enhances GPP through extended growing seasons (Zhang H et al., 2018) and enhanced vegetation greening (Luo et al., 2020; Wang et al., 2021), yet may induce stress in warm-humid regions through such as increased vapor pressure deficit (VPD) (Piao et al., 2019; Chen et al., 2020). Similarly, while precipitation alleviates drought, it can suppress growth through reduced solar radiation and intensified soil erosion (Liu et al., 2018). It is therefore imperative to assess differences in temperature-precipitation controls on long-term trends and interannual variability of GPP in the TP. Crucially, under the unique westerly-monsoon synergy shaping distinct climatic zones, whether dominant climatic drivers of GPP diverge across these subregions remains unclear.

To address these issues, this study aims to: (1) quantify the relative regional contributions of the monsoon, transition, and westerlies zones to Tibetan Plateau-wide (TP-wide) GPP long-term trend and IAV; (2) identify the dominant climatic drivers of GPP trends and IAV across the TP; (3) compare differences in the primary drivers of GPP changes among distinct climatic subregions. Achieving these objectives will clarify climatic controls of TP GPP across temporal scales

under westerlies and monsoon synergy, providing a scientific basis for ecological management and sustainable development goal (SDG) achievement.

2. Data and methods

2.1 Study area and climatic zones

The TP boundary follows Zhang Y L et al. (2021), determined by geomorphological and geological evolution criteria. The TP spans 25°59′30″N–40°01′00″N and 67°40′37″E–104°40′57″E, extending across multiple countries/regions including China. Climatic zones were delineated according to Huang et al. (2023): regions north of the northernmost limit of interannual fluctuation of 300 mm annual precipitation isoline were classified as the westerlies zone; regions south of the southernmost limit were designated the monsoon zone; and the transition zone was defined as the belt between these limits.

2.2 Data

The GLASS (global land surface satellite) GPP product is derived from a revised eddy covariance-light use efficiency (EC-LUE) model, which integrates the effects of atmospheric CO₂ concentration, direct and diffuse radiation, and VPD on GPP (Zheng et al., 2020). Generally, the GLASS product could effectively capture the spatial, seasonal, and interannual variations of GPP and has been widely applied to evaluate GPP dynamics across multiple spatiotemporal scales (Liang et al., 2023). To assess the robustness of our findings, we additionally employed an alternative GIMMS (global inventory modeling and mapping studies) GPP product. This dataset is based on an optimized LUE model that integrates flux tower observations, GIMMS3g canopy photosynthetically active radiation (PAR), and meteorological data (Madani et al., 2017).

To evaluate terrestrial ecosystem models' capability in reproducing regional contributions and dominant climatic drivers of long-term trend and IAV of GPP across the TP, we utilized gridded GPP estimates from 16 dynamic global vegetation models (DGVMs) participating in the TRENDY-v11 (trends in net land atmosphere carbon exchange) project. These models include: CABLE-POP, CLASSIC, CLM5.0, IBIS, ISAM, ISBA-CTRIP, JSBACH, JULES, LPJwsl, LPX-Bern, OCN, ORCHIDEE, SDGVM, VISIT, VISIT-NIES, and YIBs. Each DGVM performed four simulation experiments (S0, S1, S2, S3). The simulation S3, which was forced by time-varying atmospheric CO₂ concentration, nitrogen deposition, climate change, and land use/cover (Zhu et al., 2016), was selected for subsequent analyses in this study.

Temperature and precipitation data were obtained from the

CRU JRA v2.5 dataset, which combines reanalysis data from Japanese Meteorological Agency with adjustment to align with the CRU TS 4.08 data as possible (Harris et al., 2020). To facilitate cross-dataset analysis, all datasets were regridded to a uniform 0.1°×0.1° resolution. Annual data were derived for the period 1982–2018.

2.3 Methods

2.3.1 Regional contribution

Contributions of the monsoon, transition, and westerlies zones to TP-wide mean-state GPP are defined as the ratio of the multi-year mean GPP within each subregion to mean GPP across the entire TP. Long-term trend of GPP were estimated via univariate linear regression using least-squares. Contribution of each subregion to TP-wide GPP trend is expressed as the ratio of its subregional GPP trend to the TP-wide GPP trend. Relative contribution to GPP IAV were quantified following Ahlström et al. (2015):

$$f_{j} = \frac{\sum_{t} \frac{x_{jt} |X_{t}|}{X_{t}}}{\sum_{t} |X_{t}|},$$
(1)

where x_{jt} is the GPP anomaly for subregion j at time t (relative to its long-term trend), X_t is the TP-wide GPP anomaly at time t, calculated as $\sum_j x_{jt}$, $|X_t|$ is the absolute magnitude of the TP-wide GPP anomaly, serving as the weighting factor, and f_j denotes the relative contribution of subregion j to TP-wide GPP IAV. Subregion with higher positive value of f_j indicates stronger contributions to TP-wide IAV.

2.3.2 Climate attribution

Contribution of climate factor (temperature or precipitation) to the GPP trend was calculated as the product of the observed trend in each variable and its corresponding regression coefficient derived from the multiple linear regression model (eq. (2)):

$$GPP = b_1 \times Tas + b_2 \times Pre + b_0, \tag{2}$$

where Tas is the annual mean temperature, Pre is the annual precipitation, b_1 and b_2 are the regression coefficients estimated via least-squares regression, representing the sensitivity of GPP to temperature and precipitation, respectively. Uncertainty in contribution estimates of each climatic variable was quantified using the 95% confidence interval of its respective regression coefficient.

To examine the relative importance of temperature and precipitation in driving GPP IAV, we employed a percentile-based approach (Liu et al., 2020), which isolates the individual effects of climatic drivers by leveraging their relative decoupling within specific bins. Prior to analysis, all variables were linearly detrended and standardized via

z-score transformation (i.e., mean-centered and scaled by their standard deviations), ensuring dimensionless comparability across grid cells or subregions. We sort temperature and precipitation into 10 bins (0%–10%, 10%–20%, ..., 90%–100%) according to the thresholds at the 10th, 20th, ..., 90th percentiles. Within each precipitation bin (i=1, 2, ..., 10), temperature was further resorted. The effect of temperature on GPP ($\Delta GPP(Tas|Pre)$) was then quantified as the difference in GPP between the highest and lowest temperature bin in each precipitation bin as follows (eq. (3)):

$$\Delta GPP(Tas|Pre) = \frac{1}{I} \sum_{i=1}^{I} GPP_{i,n_{i,\text{max}}} - GPP_{i,n_{i,\text{min}}},$$
 (3)

where I is the number of precipitation bins, i denotes the specific precipitation bin, $n_{i,\max}$ and $n_{i,\min}$ are the maximum and minimum temperature bin numbers at precipitation bin i, respectively, and $GPP_{i,n_{i,\max}}$ and $GPP_{i,n_{i,\min}}$ are the average GPP for the highest and lowest temperature bin within precipitation bin i. Similarly, the effect of precipitation on GPP ($\Delta GPP(Pre|Tas)$) was computed as the GPP difference between the highest and lowest precipitation bin within each temperature bin (eq. (4))

$$\Delta GPP(Pre|Tas) = \frac{1}{J} \sum_{i=1}^{J} GPP_{j,n_{j,\text{max}}} - GPP_{j,n_{j,\text{min}}}, \tag{4}$$

where J is the number of temperature bin, j denotes the specific temperature bin, and $GPP_{j,n_{j,\max}}$ and $GPP_{j,n_{j,\min}}$ are the average GPP for the highest and lowest precipitation bin in temperature bin j. Only bins containing at least 10 data points were included in the analysis to ensure robustness.

3. Results

3.1 Regional contributions to long-term trend and interannual variability of GPP across the Tibetan Plateau

Based on the GLASS dataset, the mean annual GPP across the TP was 1012.91 Tg C a⁻¹ from 1982 to 2018. Spatially, GPP exhibited pronounced heterogeneity, characterized by a distinct southeast-to-northwest decreasing gradient (Figure 1a). The southeastern monsoon zone, benefiting from favorable hydrothermal conditions, displayed the highest GPP values (>1400 g C m⁻²). Notably, another high-GPP region occurred along the southwestern frontier (Appendix Figure S1), where forest cover prevails. Conversely, the westerlies zone in the northern TP, dominated by alpine desert, showed the lowest GPP (<150 g C m⁻²). When partitioning TP-wide GPP among the subregions, we found that the monsoon zone contributed the largest proportion of annual GPP (86.07%, 871.85 Tg C a^{-1}) during 1982–2018, followed by the transition zone (10.04%, 101.71 Tg C a⁻¹), while the westerlies zone accounted for the smallest proportion (3.89%, 39.35 Tg C a⁻¹) (Figure 2).

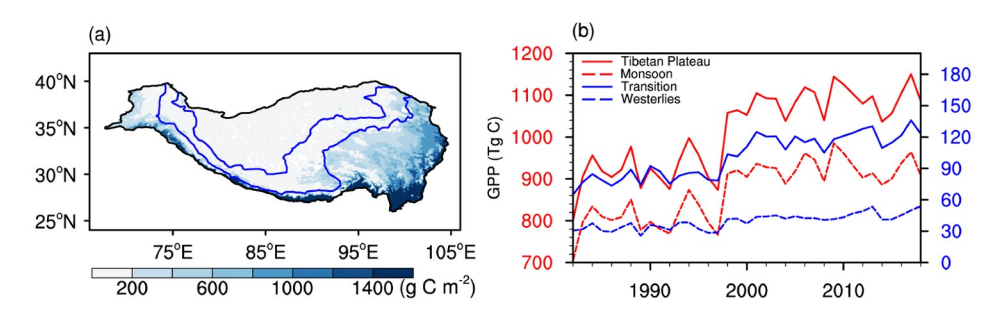


Figure 1 Spatial pattern and interannual trends of GPP across the Tibetan Plateau during 1982–2018. (a) Spatial distribution of multi-year mean GPP. Blue lines delineate boundaries of climatic subregions defined by the 300 mm annual precipitation isoline. (b) Time series of annual total GPP for the entire Tibetan Plateau, and the monsoon, transition, and westerlies zones.

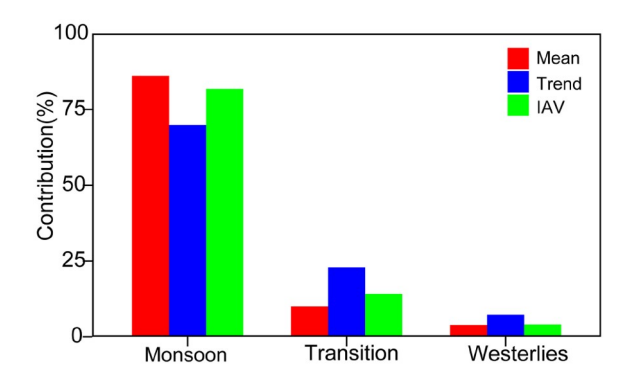


Figure 2 Relative contributions of the monsoon, transition, and westerlies zones to the mean state, long-term trend, and interannual variability (IAV) of plateau-wide GPP.

Annual GPP across the TP increased significantly at 7.32 Tg C a^{-2} (p<0.01) during the study period (Figure 1b). Although the monsoon zone dominated the positive TP-wide trend (69.84%, 5.11 Tg C a^{-2}), its relative contribution was 16.23% lower than its proportion to the mean-state GPP. In contrast, both the transition (22.88%) and the westerlies zone (7.28%) exhibited increased contributions to the GPP trend relative to their mean-state proportions (Figure 2).

Using eq. (1), we quantified each subregional contribution to TP-wide GPP IAV. Unlike standard deviation—which measures absolute variability of GPP within subregions—this metric assesses the relative importance of each subregion in governing the IAV of the TP-wide GPP. Results indicate that the monsoon zone dominated TP-wide GPP IAV (81.80%), followed by the transition zone (14.17%) and westerlies zone (4.03%) (Figure 2). Notably, both transition and westerlies zones contributed more to TP-wide GPP IAV relative to mean-state GPP, with increases of 4.13% and 0.14%, respectively.

3.2 Relative contribution of temperature and precipitation on long-term GPP trends across the Tibetan Plateau and its subregions

During 1982–2018, the annual mean temperature over the TP

exhibited a significant increasing trend, with warming rates exceeding 0.2°C (10 a)⁻¹ across most areas. Precipitation increased overall, with the strongest increase occurring in the transition zone; however, parts of the monsoon and westerlies zones showed decreasing trends (Appendix Figure S2). The relative contributions of temperature and precipitation to GPP trends were determined by their respective GPP sensitivities and temporal trends. At the grid scale, temperature dominated GPP trends in >90% of areas. Although its contribution was relatively lower in the transition zone than in other subregions, it remained the dominant driver there (Figure 3a). Regionally, the significant TP-wide GPP increase was primarily driven by rising annual mean temperature, accounting for 80.29%±15.77% of the trend (Figure 3b). In the monsoon zone, temperature contributed $77.88\% \pm 15.93\%$ to the GPP trend (5.11 Tg C a⁻²). Temperature dominates GPP trends here because summer maximum temperatures remain below the 13°C optimum for vegetation productivity (Huang et al., 2019), making it the primary constraint on long-term growth. Similarly, temperature dominated GPP increases in the transition (57.26% ±19.24%) and westerlies zone (71.35%±22.73%). Precipitation played a negligible role in the monsoon zone $(\sim 0\%)$ but had greater importance in the transition (9.53%) $\pm 12.75\%$) and westerlies zones (6.70% $\pm 13.74\%$), reflecting stronger moisture limitation in these arid regions.

3.3 Relative importance of temperature and precipitation on interannual variability of GPP across the Tibetan Plateau and its subregions

We analyzed the relative importance of temperature and precipitation in driving GPP IAV using a percentile-based binning approach. Within fixed precipitation bins, higher temperatures enhance GPP across the TP, whereas GPP showed negligible responsiveness to increasing precipitation within fixed temperature bins (Figure 4b). Consistently, the temperature effect ($\Delta GPP(Tas|Pre)$) averaged 0.46 standard deviation (SD), significantly exceeding the precipitation effect ($\Delta GPP(Pre|Tas)$ =0.01 SD) (Figure 4c), establishing

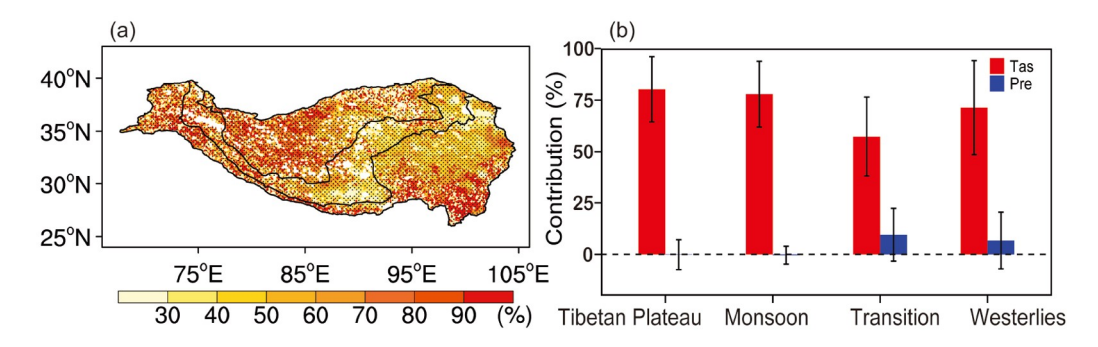


Figure 3 Relative contributions of temperature to the long-term GPP trend at (a) grid and (b) subregional scales. Stippled areas in (a) denote grids where temperature is the dominant driver of GPP trends. Error bars in (b) indicate 90% confidence intervals.

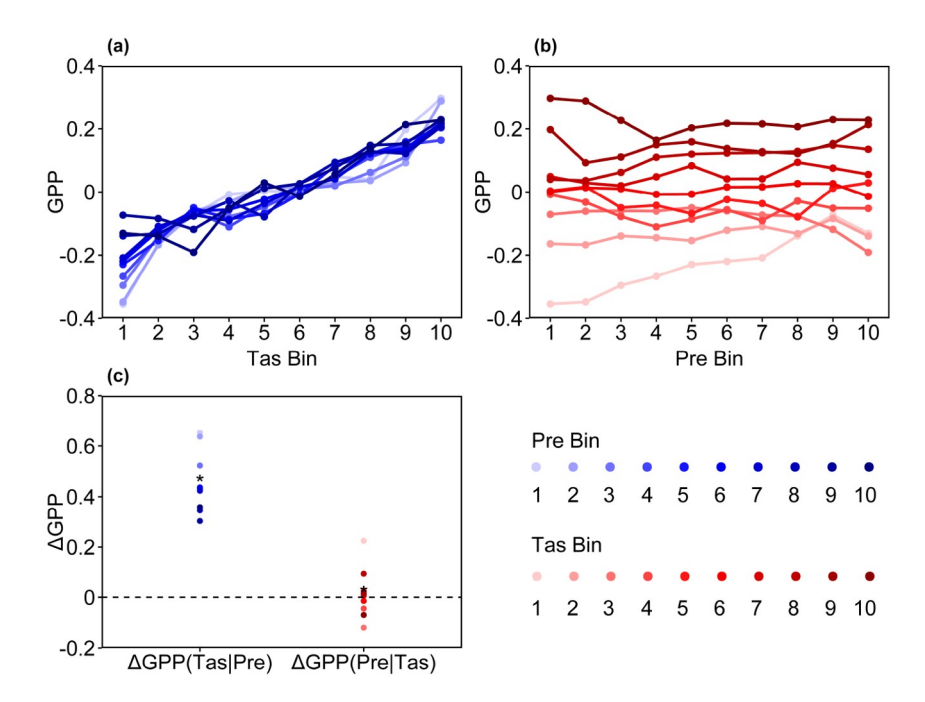


Figure 4 Relative importance of temperature and precipitation to GPP interannual variability across the entire Tibetan Plateau. (a) GPP response to temperature variability binned by precipitation percentiles. (b) GPP response to precipitation variability binned by temperature percentiles. (c) Distributions of $\Delta GPP(Tas|Pre)$ and $\Delta GPP(Tre|Tas)$. Asterisks (*) denote the corresponding mean values across all bins.

temperature as the dominant TP-wide driver.

In the monsoon zone, GPP increased with temperature within fixed precipitation bins (Figure 5a), with $\Delta GPP(Tas|Pre)$ averaging 0.63 SD (Figure 5c). Conversely, precipitation exerted minimal influence on GPP ($\Delta GPP(Pre|Tas)$ =-0.03 SD; Figure 5b). Given this region's dominant contribution (81.80%) to TP-wide GPP IAV (Figure 2), its temperature-driven variability explains the observed plateau-wide thermal control. Notably, precipitation suppressed GPP IAV at high temperature quantiles (90th-100th percentiles; Figure 5b), likely due to radiation limitation on photosynthesis under increased precipitation (Xiong et al., 2021).

In the transition zone, GPP responded positively to both drivers (Figure 6a, 6b), but temperature dominance persisted

($\Delta GPP(Tas|Pre)$ =0.30 SD vs. $\Delta GPP(Pre|Tas)$ =0.13 SD; Figure 6c). However, precipitation's relative importance was amplified compared with the monsoon zone, despite remaining secondary to temperature. This shift reflects constrained water availability in these drier conditions, resulting in greater vegetation sensitivity to moisture variations.

For the westerlies zone, GPP generally increased with rising temperature within precipitation bins (mean $\Delta GPP(Tas|Pre)=0.30$ SD; Figure 7a, 7c), indicating thermal dominance due to physiological constraints imposed by high-altitude cooling. Conversely, precipitation exerted weak overall effects, even with GPP declining beyond the 80th percentile (Figure 7b). This suppression may be attributed to the prevalence of alpine desert (Appendix Figure S1), where the shallow-rooted *Ceratoides compacta* dom-

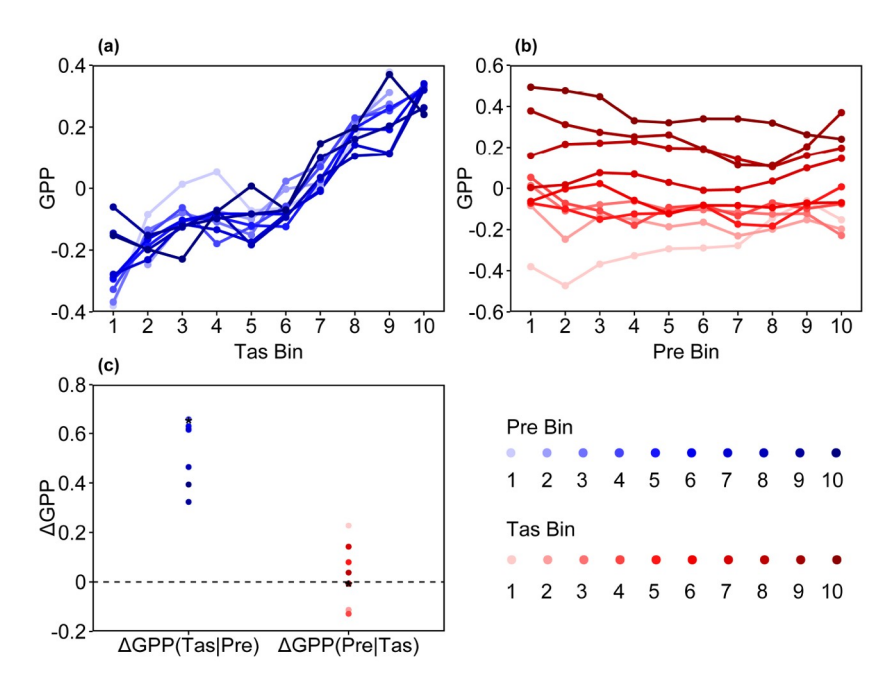


Figure 5 Relative importance of temperature and precipitation to GPP interannual variability in the monsoon zone. (a) GPP response to temperature variability binned by precipitation percentiles. (b) GPP response to precipitation variability binned by temperature percentiles. (c) Distributions of $\Delta GPP(Tas|Pre)$ and $\Delta GPP(Pre|Tas)$. Asterisks (*) denote the corresponding mean values across all bins.

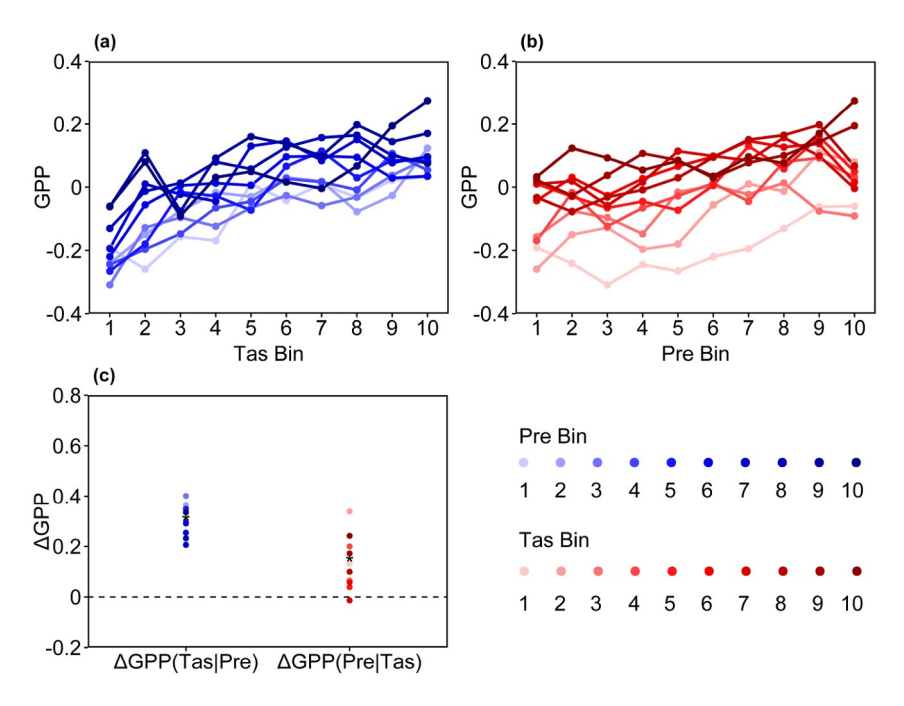


Figure 6 Relative importance of temperature and precipitation to GPP interannual variability in the transition zone. (a) GPP response to temperature variability binned by precipitation percentiles. (b) GPP response to precipitation variability binned by temperature percentiles. (c) Distributions of $\Delta GPP(Tas|Pre)$ and $\Delta GPP(Pre|Tas)$. Asterisks (*) denote the corresponding mean values across all bins.

inates (Zhao et al., 2017). When precipitation exceeds a certain threshold, excessive moisture can exacerbate soil anoxia, amplify erosion-driven nutrient loss, and reduce soil organic matter, collectively limiting photosynthesis and depressing GPP (Peng et al., 2024).

4. Discussion and conclusions

Quantitative assessment based on the GLASS dataset demonstrates that the monsoon zone contributed 86.07%, 69.84%, and 81.80% to the mean-state, long-term trend, and

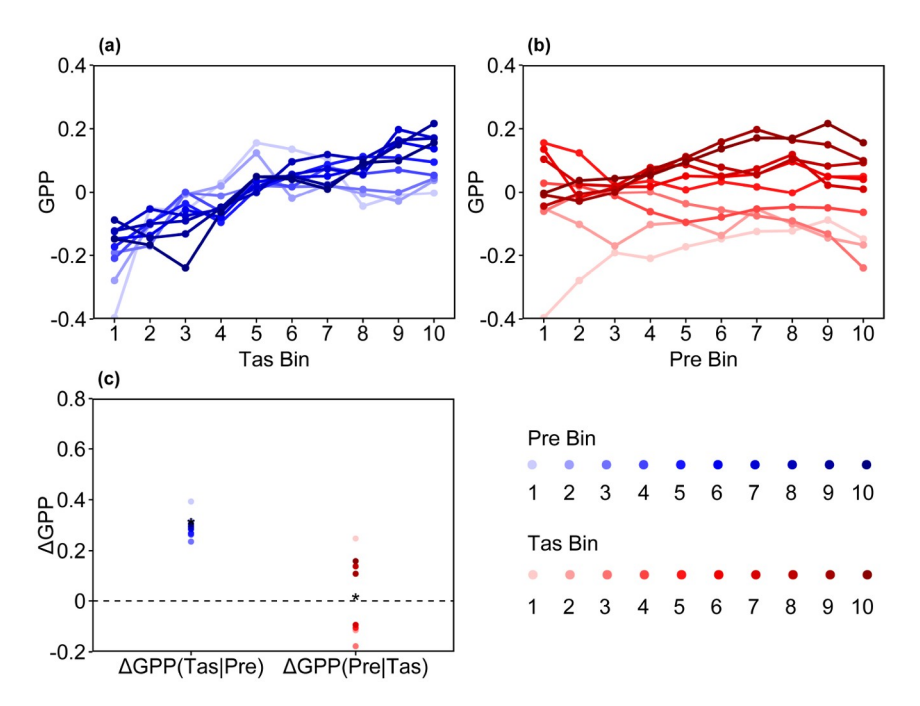


Figure 7 Relative importance of temperature and precipitation to GPP interannual variability in the westerlies zone. (a) GPP response to temperature variability binned by precipitation percentiles. (b) GPP response to precipitation variability binned by temperature percentiles. (c) Distributions of $\Delta GPP(Tas|Pre)$ and $\Delta GPP(Pre|Tas)$. Asterisks (*) denote the corresponding mean values across all bins.

IAV of the TP-wide GPP, respectively. Corresponding contributions from the transition zone were 10.04%, 22.88%, and 14.17%, while the westerlies zone accounted for 3.89%, 7.28%, and 4.03% (Figure 2). Although the monsoon zone dominated TP-wide GPP dynamics across temporal scales, its proportional contributions to long-term trends and IAV were lower than to the mean state, highlighting non-negligible roles of the transition and westerlies zones in temporal GPP evolution of TP. To evaluate the robustness of these findings, we performed a comparative analysis using the GIMMS dataset (1982-2016). Results revealed consistent spatial divergence patterns across datasets: both the transition and westerlies zones exhibited larger contributions to the long-term trend and IAV than to the mean-state, whereas the monsoon zone showed reduced proportions (Appendix Figure S3). Multi-model ensemble mean from TRENDY was further validated these conclusions (Figure 8). However, inter-model discrepancies existed due to differences in model structures and parameterization schemes. For example, IBIS, JULES, and ORCHIDEE simulated higher monsoon zone contributions to the GPP trend than to the mean state. JSBACH indicated a greater monsoon zone contribution to GPP IAV compared to the mean state, but lower contributions to the long-term trend.

Long-term vegetation dynamics under climate change involve complex processes, particularly for sensitive and fragile ecosystems such as the TP. Based on the GLASS dataset, significant GPP increase across the monsoon, transition, and westerlies zones during 1982–2018 were predominantly

driven by temperature, accounting for 77.88%±15.93%, 57.26%±19.24%, and 71.35%±22.73% of these trends, respectively. The findings were further corroborated by analyses using GIMMS (Appendix Figure S4) and TRENDY (Figure 9) datasets. Notably, studies utilizing vegetation indices (e.g., greenness) as response variables identified annual precipitation as the primary driver of vegetation changes (Chang et al., 2023). This apparent contradiction likely results from the decoupling GPP dynamics from greenness indices (e.g., LAI) across the TP, modulated by spatial heterogeneity in water availability, vegetation structure, and canopy density (An et al., 2024).

This study demonstrates that temperature dominates TPwide GPP IAV, consistent with documented heightened temperature sensitivity of plateau vegetation photosynthesis (Zeng and Yang, 2008; Zhang Q et al., 2018; Zhang X et al., 2021). When focusing on subregions, temperature controls GPP IAV in the monsoon zone where widespread rainfall transported by summer monsoon moisture from the Bay of Bengal and Arabian Sea-effectively eliminates water stress. In these energy-limited ecosystems, moderate warming enhances Rubisco activity and extends the growing season, while concomitant increased light availability further promotes photosynthetic efficiency, jointly boosting GPP. Precipitation exerted minimal influence on GPP IAV in the monsoon zone. Eddy covariance-based studies corroborate the absence of a significant precipitation-GPP relationship in alpine meadows (Guo et al., 2015). Notably, even a slight negative contribution of precipitation to GPP IAV can be

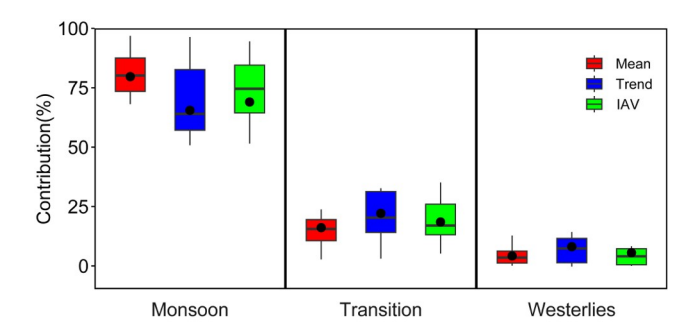


Figure 8 TRENDY-based relative contributions of climatic subregions (the monsoon, transition, and westerlies zones) to plateau-wide GPP characteristics based on TRENDY-v11 models: (left) mean state, (middle) long-term trend, (right) interannual variability. Boxes show 5th–95th percentiles of 16 models. Black dots represent multi-model ensemble means.

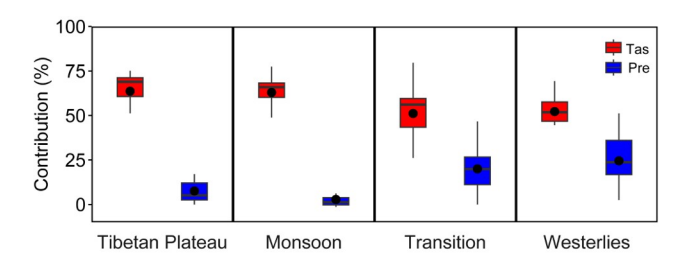


Figure 9 TRENDY-based relative contributions of temperature and precipitation to the long-term GPP trend across the entire Tibetan Plateau and the monsoon, transition, and westerlies zones. Boxes show 90% confidence intervals. Black dots indicate multi-model ensemble means.

found in the higher temperature bins. This suppression is likely attributable to radiation limitation under cloudy conditions and impaired soil oxygen diffusion associated with increased precipitation. In the transition and westerlies zone, temperature persists as the primary driver of GPP IAV, contrasting with some studies emphasizing precipitation dominance in semi-arid/arid climate zones (Hu et al., 2023). Although precipitation's relative contribution increased in the transition zone relative to the monsoon, it did not surpass thermal dominance. In the westerlies region, chronically low temperatures (Zeng and Yang, 2008) impose fundamental

physiological constraints on vegetation growth. Critically, GIMMS-based analysis confirms pervasive temperature control of GPP IAV across all subregions (Appendix Figures S5–S8).

In contrast to satellite-derived observations, the TRENDY multi-model ensemble mean indicates precipitation-dominated GPP IAV across all subregions (Figure 10), with the strongest precipitation control observed in the transition zone. The failure of process-based terrestrial ecosystem models to reproduce observed climate-GPP IAV relationships may stem from the following limitations: First, current models inadequately represent permafrost-vegetation coupling mechanisms. Approximately 41%-64% of the TP is underlain by permafrost (Peng et al., 2023), where freezethaw cycles exert complex trade-offs on vegetation dynamics. Initial degradation may enhance vegetation productivity by improving soil moisture and nutrient availability (Shi et al., 2023), whereas sustained degradation disrupts soil hydrology, accelerating drainage and evaporation that desiccate surface soils and trigger degradation of shallowrooted vegetation (Wang and Liu, 2022; Zhu et al., 2022). Nevertheless, the absence of explicit representations of vegetation responses to permafrost dynamics in the ecosystem models severely limits their applicability for simulating the TP carbon cycle (McGuire et al., 2018). Second, the lack of plateau-specific parameter values undermines model performance. Ecosystem models require spatially calibrated parameters to capture ecological heterogeneity, yet extreme conditions on the TP restrict the availability of ground validation data—primarily from low-elevation sites—which impairs model upscaling to high-altitude zones and introduces systematic biases (Ma et al., 2018). For instance, vegetation adapts to low CO₂ partial pressure at high elevations through increased Vcmax (Fan et al., 2011). Similarly, parameters in empirical stomatal models (e.g., Ball-Berry) exhibit elevation-dependent variations due to their tight coupling with temperature and moisture deficit (Körner et al., 1986; Lin et al., 2015). Particularly on the TP, spatial

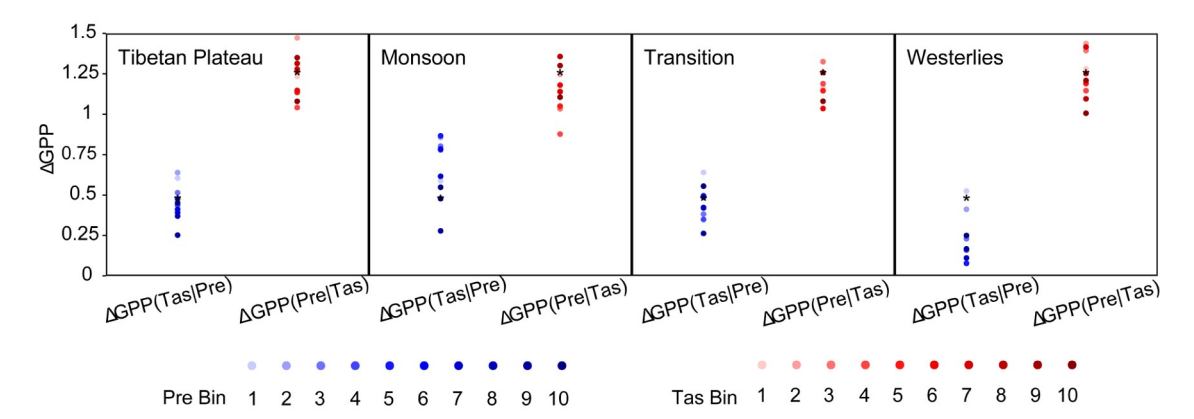


Figure 10 Distributions of $\triangle GPP(Tas|Pre)$ and $\triangle GPP(Pre|Tas)$ across the entire Tibetan Plateau, and the monsoon, westerlies, and transition zones derived from multi-model ensemble means of TRENDY. Asterisks (*) denote the corresponding mean values across all bins.

heterogeneity persists in parameters even within the same vegetation type (Ma et al., 2025). Furthermore, models incorporating carbon-nitrogen interactions and atmospheric nitrogen deposition generally exhibit improved performance. Although most terrestrial ecosystem models in the TRENDY project include these mechanisms (Friedlingstein et al., 2022), inadequate representation of processes—particularly the regulation of nitrogen limitation strength on carbon uptake—constitutes a source of simulation bias (Zaehle et al., 2014).

This study focused on the impacts of two typical climatic factors, temperature and precipitation, on vegetation productivity across the TP. It should be noted that the regulatory effects of other factors on GPP—such as CO₂ (Luo et al., 2020), radiation (Wei et al., 2022), nitrogen deposition (Chen et al., 2022), and human activities (Xiong et al., 2021)—were not considered in the current research scope. Furthermore, our analysis centered on annual-scale meteorological variables to identify the dominant drivers of GPP IAV. However, emerging evidence suggests that interannual fluctuations in vegetation GPP may correlate more strongly with meteorological changes during specific periods. That is, seasonal variations in climatic drivers are more important for GPP IAV than variations in annual climate conditions, potentially serving as more significant determinants (Baldocchi et al., 2018). Therefore, future studies urgently need to integrate climatic factors at higher temporal resolutions and incorporate a broader range of environmental variables to advance our mechanistic understanding of carbon cycle processes within the TP ecosystem.

Acknowledgements We thank the TRENDY team for making their data available. This work was supported by the Second Tibetan Plateau Scientific Expedition and Research Program (Grant No. 2019QZKK0106) and the National Natural Science Foundation of China (Grant No. 42141007).

Conflict of interest The authors declare no conflict of interest.

Supporting information The supporting information is available online at http://earth.scichina.com and http://earth.scichina.com and http://earth.scichina.com and http://earth.scichina.com and http://earth.scichina.com and http://earth.scichina.com and <a href="http:/

References

- Ahlström A, Raupach M R, Schurgers G, Smith B, Arneth A, Jung M, Reichstein M, Canadell J G, Friedlingstein P, Jain A K, Kato E, Poulter B, Sitch S, Stocker B D, Viovy N, Wang Y P, Wiltshire A, Zaehle S, Zeng N. 2015. The dominant role of semi-arid ecosystems in the trend and variability of the land CO₂ sink. Science, 348: 895–899
- An R, Jin H, Zhao H, Wei D, Zhao W, Wang X. 2024. Productivity experienced a more rapid enhancement trend than greenness across the Tibetan Plateau. Sci Total Environ, 954: 176666
- Baldocchi D, Chu H, Reichstein M. 2018. Inter-annual variability of net and gross ecosystem carbon fluxes: A review. Agric For Meteor, 249:

- 520-533
- Chang Y, Yang C, Xu L, Li D, Shang H, Gao F. 2023. Analysis of vegetation dynamics and driving mechanisms on the Qinghai-Tibet Plateau in the context of climate change. Water, 15: 3305
- Chen H, Ju P, Zhu Q, Xu X, Wu N, Gao Y, Feng X, Tian J, Niu S, Zhang Y, Peng C, Wang Y. 2022. Carbon and nitrogen cycling on the Qinghai-Tibetan Plateau. Nat Rev Earth Environ, 3: 701–716
- Chen J, Yan F, Lu Q. 2020. Spatiotemporal variation of vegetation on the Qinghai-Tibet Plateau and the influence of climatic factors and human activities on vegetation trend (2000–2019). Remote Sens, 12: 3150
- Fan Y, Zhong Z, Zhang X. 2011. Determination of photosynthetic parameters Vc_{max} and J_{max} for a C_3 plant (spring hulless barley) at two altitudes on the Tibetan Plateau. Agric For Meteor, 151: 1481–1487
- Friedlingstein P, Jones M W, O'Sullivan M, Andrew R M, Bakker D C E, Hauck J, Le Quéré C, Peters G P, Peters W, Pongratz J, Sitch S, Canadell J G, Ciais P, Jackson R B, Alin S R, Anthoni P, Bates N R, Becker M, Bellouin N, Bopp L, Chau T T T, Chevallier F, Chini L P, Cronin M, Currie K I, Decharme B, Djeutchouang L M, Dou X, Evans W, Feely R A, Feng L, Gasser T, Gilfillan D, Gkritzalis T, Grassi G, Gregor L, Gruber N, Gürses Ö, Harris I, Houghton R A, Hurtt G C, Iida Y, Ilyina T, Luijkx I T, Jain A, Jones S D, Kato E, Kennedy D, Klein Goldewijk K, Knauer J, Korsbakken J I, Körtzinger A, Landschützer P, Lauvset S K, Lefèvre N, Lienert S, Liu J, Marland G, McGuire P C, Melton J R, Munro D R, Nabel J E M S, Nakaoka S I, Niwa Y, Ono T, Pierrot D, Poulter B, Rehder G, Resplandy L, Robertson E, Rödenbeck C. Rosan T M. Schwinger J. Schwingshackl C. Séférian R. Sutton A J. Sweeney C, Tanhua T, Tans P P, Tian H, Tilbrook B, Tubiello F, van der Werf G R, Vuichard N, Wada C, Wanninkhof R, Watson A J, Willis D, Wiltshire A J, Yuan W, Yue C, Yue X, Zaehle S, Zeng J. 2022. Global carbon budget 2021. Earth Syst Sci Data, 14: 1917–2005
- Guo Q, Hu Z, Li S, Yu G, Sun X, Zhang L, Mu S, Zhu X, Wang Y, Li Y, Zhao W. 2015. Contrasting responses of gross primary productivity to precipitation events in a water-limited and a temperature-limited grassland ecosystem. Agric For Meteor, 214-215: 169–177
- Harris I, Osborn T J, Jones P, Lister D. 2020. Version 4 of the CRU TS monthly high-resolution gridded multivariate climate dataset. Sci Data, 7: 109
- Hu Z, Niu B, Tang J, Zhang Y, Xiang M, Zhang X. 2023. Has the dominant climatic driver for the carbon budget of alpine grassland shifted from temperature to precipitation on the Qinghai-Tibet Plateau? Remote Sens, 15: 2492
- Huang L, Chen J, Yang K, Yang Y, Huang W, Zhang X, Chen F. 2023. The northern boundary of the Asian summer monsoon and division of westerlies and monsoon regimes over the Tibetan Plateau in presentday. Sci China Earth Sci, 66: 882–893
- Huang M, Piao S, Ciais P, Peñuelas J, Wang X, Keenan T F, Peng S, Berry J A, Wang K, Mao J, Alkama R, Cescatti A, Cuntz M, De Deurwaerder H, Gao M, He Y, Liu Y, Luo Y, Myneni R B, Niu S, Shi X, Yuan W, Verbeeck H, Wang T, Wu J, Janssens I A. 2019. Air temperature optima of vegetation productivity across global biomes. Nat Ecol Evol, 3: 772–779
- Körner C, Bannister P, Mark A F. 1986. Altitudinal variation in stomatal conductance, nitrogen content and leaf anatomy in different plant life forms in New Zealand. Oecologia, 69: 577–588
- Lin Y S, Medlyn B E, Duursma R A, Prentice I C, Wang H, Baig S, Eamus D, de Dios V R, Mitchell P, Ellsworth D S, de Beeck M O, Wallin G, Uddling J, Tarvainen L, Linderson M L, Cernusak L A, Nippert J B, Ocheltree T W, Tissue D T, Martin-StPaul N K, Rogers A, Warren J M, De Angelis P, Hikosaka K, Han Q, Onoda Y, Gimeno T E, Barton C V M, Bennie J, Bonal D, Bosc A, Löw M, Macinins-Ng C, Rey A, Rowland L, Setterfield S A, Tausz-Posch S, Zaragoza-Castells J, Broadmeadow M S J, Drake J E, Freeman M, Ghannoum O, Hutley L B, Kelly J W, Kikuzawa K, Kolari P, Koyama K, Limousin J M, Meir P, Lola da Costa A C, Mikkelsen T N, Salinas N, Sun W, Wingate L. 2015. Optimal stomatal behaviour around the world. Nat Clim Change, 5: 459–464
- Li L, Zhang R, Wen M, Lv J. 2021. Regionally different precipitation trends over the Tibetan Plateau in the warming context: A perspective

- of the Tibetan Plateau vortices. Geophys Res Lett, 48: e2020GL091680 Li X, Ma H, Ran Y, Wang X, Zhu G, Liu F, He H, Zhang Z, Huang C. 2021. Terrestrial carbon cycle model-data fusion: Progress and challenges. Sci China Earth Sci, 64: 1645–1657
- Liang S, Chen X, Chen Y, Cheng J, Jia K, Jiang B, Li B, Liu Q, Ma H, Song L, Tang B, Xu J, Yao Y, Yuan W, Zhang X, Zhang Y, Zhao X, Zhou J. 2023. Updates on Global LAnd Surface Satellite (GLASS) products suite (in Chinese). Natl Remote Sens Bull, 27: 831–856
- Liu D, Li Y, Wang T, Peylin P, MacBean N, Ciais P, Jia G, Ma M, Ma Y, Shen M, Zhang X, Piao S. 2018. Contrasting responses of grassland water and carbon exchanges to climate change between Tibetan Plateau and Inner Mongolia. Agric For Meteor, 249: 163–175
- Liu L, Gudmundsson L, Hauser M, Qin D, Li S, Seneviratne S I. 2020. Soil moisture dominates dryness stress on ecosystem production globally. Nat Commun, 11: 4892
- Liu Y, Chen H, Li H, Zhang G, Wang H. 2021. What induces the interdecadal shift of the dipole patterns of summer precipitation trends over the Tibetan Plateau? Intl J Climatol, 41: 5159–5177
- Luo X, Jia B, Lai X. 2020. Contributions of climate change, land use change and CO₂ to changes in the gross primary productivity of the Tibetan Plateau. Atmos Ocean Sci Lett, 13: 8-15
- Ma C, Duan S B, Xu C, Qin W, Wang F, He L. 2025. Spatio-temporal simulation of net ecosystem productivity in the Tibetan Plateau region using multi-scale data assimilation for terrestrial ecosystem process model. Agric For Meteor, 366: 110471
- Ma M, Yuan W, Dong J, Zhang F, Cai W, Li H. 2018. Large-scale estimates of gross primary production on the Qinghai-Tibet plateau based on remote sensing data. Int J Digital Earth, 11: 1166–1183
- Madani N, Kimball J S, Running S W. 2017. Improving global gross primary productivity estimates by computing optimum light use efficiencies using flux tower data. J Geophys Res Biogeosci, 122: 2939– 2951
- Maussion F, Scherer D, Mölg T, Collier E, Curio J, Finkelnburg R. 2014.Precipitation seasonality and variability over the Tibetan Plateau as resolved by the high Asia reanalysis. J Clim, 27: 1910–1927
- McGuire A D, Lawrence D M, Koven C, Clein J S, Burke E, Chen G, Jafarov E, MacDougall A H, Marchenko S, Nicolsky D, Peng S, Rinke A, Ciais P, Gouttevin I, Hayes D J, Ji D, Krinner G, Moore J C, Romanovsky V, Schädel C, Schaefer K, Schuur E A G, Zhuang Q. 2018. Dependence of the evolution of carbon dynamics in the northern permafrost region on the trajectory of climate change. Proc Natl Acad Sci USA, 115: 3882–3887
- Peng J, Tang J, Xie S, Wang Y, Liao J, Chen C, Sun C, Mao J, Zhou Q, Niu S. 2024. Evidence for the acclimation of ecosystem photosynthesis to soil moisture. Nat Commun, 15: 9795
- Peng X Q, Tian W W, Li X J, Yang G S, Zhao Y H, Chen C, Jin H D, Luo J, Li Y X, Sun W, Wand Q F, Frauenfeld Q W, Mou C C. Research progress on changes in frozen ground on the Qinghai-Tibet Plateau and in the circum-Arctic region (in Chinese). J Glaciol Geocryol, 2023, 45: 521–534
- Piao S L, Zhang X Z, Wang T, Liang E Y, Wang S P, Zhu J T, Niu B. 2019. Responses and feedback of the Tibetan Plateau's alpine ecosystem to climate change. Chin Sci Bull, 64: 2842–2855
- Shi S, Wang P, Zhan X, Han J, Guo M, Wang F. 2023. Warming and increasing precipitation induced greening on the northern Qinghai-Tibet Plateau. Catena, 233: 107483
- Wang J, Liu D. 2022. Vegetation green-up date is more sensitive to permafrost degradation than climate change in spring across the northern permafrost region. Glob Change Biol, 28: 1569–1582
- Wang Z, Cui G, Liu X, Zheng K, Lu Z, Li H, Wang G, An Z. 2021. Greening of the Qinghai-Tibet Plateau and its response to climate variations along elevation gradients. Remote Sens, 13: 3712
- Wei J, Li X, Liu L, Christensen T R, Jiang Z, Ma Y, Wu X, Yao H, López-Blanco E. 2022. Radiation, soil water content, and temperature effects on carbon cycling in an alpine swamp meadow of the northeastern Qinghai-Tibetan Plateau. Biogeosciences, 19: 861–875

- Wu J, Li M, Zhang X, Fiedler S, Gao Q, Zhou Y, Cao W, Hassan W, Mărgărint M C, Tarolli P, Tietjen B. 2021. Disentangling climatic and anthropogenic contributions to nonlinear dynamics of alpine grassland productivity on the Qinghai-Tibetan Plateau. J Environ Manage, 281: 111875
- Xiong Q, Xiao Y, Liang P, Li L, Zhang L, Li T, Pan K, Liu C. 2021. Trends in climate change and human interventions indicate grassland productivity on the Qinghai-Tibetan Plateau from 1980 to 2015. Ecol Indicators, 129: 108010
- Yao T, Thompson L, Yang W, Yu W, Gao Y, Guo X, Yang X, Duan K, Zhao H, Xu B, Pu J, Lu A, Xiang Y, Kattel D B, Joswiak D. 2012. Different glacier status with atmospheric circulations in Tibetan Plateau and surroundings. Nat Clim Change, 2: 663–667
- Yao T, Masson-Delmotte V, Gao J, Yu W, Yang X, Risi C, Sturm C, Werner M, Zhao H, He Y, Ren W, Tian L, Shi C, Hou S. 2013. A review of climatic controls on δ^{18} O in precipitation over the Tibetan Plateau: Observations and simulations. Rev Geophys, 51: 525–548
- Yao Y, Wang X, Li Y, Wang T, Shen M, Du M, He H, Li Y, Luo W, Ma M, Ma Y, Tang Y, Wang H, Zhang X, Zhang Y, Zhao L, Zhou G, Piao S. 2018. Spatiotemporal pattern of gross primary productivity and its covariation with climate in China over the last thirty years. Glob Change Biol, 24: 184–196
- You Q, Cai Z, Pepin N, Chen D, Ahrens B, Jiang Z, Wu F, Kang S, Zhang R, Wu T, Wang P, Li M, Zuo Z, Gao Y, Zhai P, Zhang Y. 2021.
 Warming amplification over the Arctic Pole and Third Pole: Trends, mechanisms and consequences. Earth-Sci Rev. 217: 103625
- Zaehle S, Medlyn B E, De Kauwe M G, Walker A P, Dietze M C, Hickler T, Luo Y, Wang Y, El-Masri B, Thornton P, Jain A, Wang S, Warlind D, Weng E, Parton W, Iversen C M, Gallet-Budynek A, McCarthy H, Finzi A, Hanson P J, Prentice I C, Oren R, Norby R J. 2014. Evaluation of 11 terrestrial carbon-nitrogen cycle models against observations from two temperate Free-Air CO₂ Enrichment studies. New Phytol, 202: 803–822
- Zeng B, Yang T B. 2008. Impacts of climate warming on vegetation in Qaidam Area from 1990 to 2003. Environ Monit Assess, 144: 403–417
- Zhang H, Fan J, Wang J, Cao W, Harris W. 2018. Spatial and temporal variability of grassland yield and its response to climate change and anthropogenic activities on the Tibetan Plateau from 1988 to 2013. Ecol Indicators, 95: 141–151
- Zhang Q, Kong D, Shi P, Singh V P, Sun P. 2018. Vegetation phenology on the Qinghai-Tibetan Plateau and its response to climate change (1982– 2013). Agric For Meteor, 248: 408–417
- Zhang W, Zhou T, Zhang L. 2017. Wetting and greening Tibetan Plateau in early summer in recent decades. J Geophys Res Atmos, 122: 5808–5822
- Zhang X, Wang J, Gao Y, Wang L. 2021. Variations and controlling factors of vegetation dynamics on the Qingzang Plateau of China over the recent 20 years. Geogr Sustainab, 2: 74–85
- Zhang Y L, Li B Y, Liu L S, Zheng D. Redetermine the region and boundaries of Tibetan Plateau (in Chinese). Geogr Res, 2021, 40: 1543– 1553
- Zhao H W, Guo K, Qiao X G, Liu C C. The ecogeographical characteristics of *Ceratoides compacta* alpine desert on the Tibetan Plateau (in Chinese). Geogr Res, 2017, 36: 2441–2450
- Zheng Y, Shen R, Wang Y, Li X, Liu S, Liang S, Chen J M, Ju W, Zhang L, Yuan W. 2020. Improved estimate of global gross primary production for reproducing its long-term variation, 1982–2017. Earth Syst Sci Data, 12: 2725–2746
- Zhu B, Zhang Z, Tian J, Kong R, Chen X. 2022. Increasing negative impacts of climatic change and anthropogenic activities on vegetation variation on the Qinghai-Tibet Plateau during 1982–2019. Remote Sens, 14: 4735.
- Zhu Z, Piao S, Myneni R B, Huang M, Zeng Z, Canadell J, Ciais P, Sitch S, Friedlingstein P, Arneth A, Cao C, Cheng L, Kato E, Koven C, Li Y, Lian X, Liu R, Mao J, Pan Y, Peng S, Peñuelas J, Poulter B, Pugh T, Stocker B, Viovy N, Wang Y, Xiao Z, Yang H, Zaehle S, Zeng N. 2016. Greening of the Earth and its drivers. Nat Clim Change, 6: 791–795